JOURNAL OF CATALYSIS 146, 136–143 (1994)

NO Reduction by CO over Rh/Al_2O_3. Effects of Rhodium Dispersion on the Catalytic Properties

J. Kašpar,* C. de Leitenburg*, P. Fornasiero,* A. Trovarelli,† and M. Graziani*

*Dipartimento di Scienze Chimiche, Università di Trieste, Via A. Valerio 38, 34127 Trieste, Italy; and †Dipartimento di Scienze e Tecnologie Chimiche, Università di Udine, Via Cotonificio 108, 33100 Udine, Italy

Received January 26, 1993; revised June 23, 1993

The effects of variation of the rhodium dispersion on the catalytic reduction of NO by CO over Rh/Al_2O_3 catalysts have been investigated. NO dissociation is promoted by an increase of metal particle size which results in an enhanced catalytic activity on a turnover basis. However, the promotional effect of the particle size on the activity strongly depends on the reaction temperature, since under reaction conditions the oxidative disruption and reductive agglomeration processes modify the rhodium particle size. These processes appear to be responsible for changes of the apparent activation energy observed around 500 K. © 1994 Academic Press, Inc.

INTRODUCTION

It is well known that the kinetics of the reduction of NO by CO carried out on single-crystal metal catalysts strongly depend on the particular crystal face investigated. Importantly, Rh catalysts supported on Al_2O_3 are characterized by lower reaction rates and higher activation energies compared with the model catalysts. For instance, Rh(111) showed an activity about two orders of magnitude higher than Al_2O_3-supported rhodium catalysts (1). It appears important, therefore, to clarify the nature of the effects which influence so heavily the intrinsic activity of supported rhodium catalysts.

Previous work showed that upon increasing the size of supported rhodium particles, a small increase of reaction rates over Rh/SiO_2 catalysts is observed (2). Recently, a 50-fold increase in the turnover numbers was reported by Oh and Eickel (3) for a Rh/Al_2O_3 catalyst as the metal dispersion was decreased from 100 to 1.7%. In their paper, the authors compare the activity of catalysts of low dispersion (D = 1.7, 4.0, 9.5, and 26.4%) with that of D = 100% dispersed catalyst, but no comparison was made for catalysts of intermediate dispersion. The structure-sensitive nature of the CO–NO reaction is generally related to the steric requirements for the NO dissociation. Studies on polycrystalline rhodium wire (4) showed that for this step, which is believed to be rate-determining on supported rhodium catalysts (5, 6) at least in the low-temperature regimes (7), the presence of more than one vacant nearest neighbor metal site is required. Consistently, over Rh(100), a lying down or highly inclined adsorbed NO species was suggested as a precursor for NO dissociation (8). An adsorbate–adsorbate interaction in the range of 0.7 nm was suggested to account for the features of the NO desorption process. Notably, by assuming a spherical geometry for the supported metal particles, simple calculations show that, for example, particles of diameter of 1.57 nm contain about 150 rhodium atoms (9) and therefore they should easily satisfy the above steric requirement. With the assumed spherical geometry for the metal particles, for such a diameter, a dispersion of 70% can be calculated. Therefore, in light of these calculations, effects of particle diameter on the rate of the CO–NO reaction might be expected also for particles of intermediate dispersion. In the present study, Al_2O_3-supported rhodium catalysts with dispersions varying between 25 and 95% were prepared and tested for the above reaction. Furthermore, the effects of particle size on the NO dissociation step were investigated by means of temperature-programmed desorption (TPD) of NO. To obtain information on the morphology of the catalysts *in situ* IR measurements were carried out as well. TPD studies show that NO dissociation is effectively enhanced by the increase of the particle size. As far as the catalytic activity is concerned, an increase of the particle size effectively promotes NO reduction by CO over the range of metal dispersions investigated; however, this occurs only above 500 K. At lower reaction temperatures such an increase is not observed. The *in situ* IR spectra suggest that this behavior may be attributed to changes in the morphology of the supported rhodium particles as a function of temperature.

EXPERIMENTAL

All the catalysts were prepared by the incipient wetness technique using $RhCl_3 \cdot 3H_2O$ (Metalli Preziosi) as metal precursor and γ-alumina (Alfa, BET surface area 99 m^2

0021-9517/94 $6.00

TABLE 1

Characteristics of the Catalyst Samples

Sample code	Rh loading[a] (wt%)	Dispersion[b] (%)	Particle diameter[c] (nm)
A	0.46	95	1.16
B	2.25	84	1.31
C	2.44	71	1.55
D	5.84	41	2.65
E	11.21	25	4.32

[a] As measured by XRF.
[b] Calculated assuming an adsorption stoichiometry H : Rh = 1 : 1.
[c] Calculated assuming spherical geometry for the metal particles.

g^{-1}) as support. After impregnation, catalysts were dried at 393 K overnight and then calcined at 623 K for 3 h. Metal loadings were measured by means of X-ray fluorescence. Hydrogen chemisorption at 298 K was measured on a Carlo Erba Sorptomatic 1900 adsorption apparatus. The amount of gas uptake was obtained by extrapolating the linear part of the adsorption isotherm to zero pressure. Rhodium loadings and the apparent Rh dispersions as measured by H_2 chemisorption are listed in Table 1.

Catalytic Tests and Temperature-Programmed Desorption

Catalytic tests were carried out at atmospheric pressure in a stainless steel flow microreactor (4.6 mm i.d., 50 mm long). Typically 25–100 mg of catalyst were loaded into the reactor and the internal dead volume was filled with granular quartz. Reduction of the catalysts was carried out *in situ* at 473 K for 30 min using a H_2/He 8.5% mixture. Catalytic measurements were carried out in the range of temperatures 473–700 K using 3% CO and 1% NO in He as background following a temperature cycle as described later and using a heating rate of 0.8 K min^{-1}. The analyses of the reactor effluents were performed with an on-line Hewlett–Packard 5890 gas chromatograph. Separation of the products was achieved on a Porapak Q and Hayesep A columns. This system enabled simultaneous detection of the reactants and reaction products, i.e., CO, CO_2, NO, N_2O, and N_2.

For the TPD experiments, 200 mg of catalyst were loaded in a quartz microreactor and reduced in H_2 (20 ml min^{-1} at 473 K for 2 h), followed by evacuation at 673 K for 2 h, and finally cooled to 298 K in a flow of He (50 ml min^{-1}). Adsorption of NO was performed at 298 K by injecting five consecutive pulses of pure NO (0.10 ml) into the He flow. Excess of NO was removed by allowing the sample to remain in the He flow until no significant amounts of NO could be detected (60 min approx.). This ensured high initial coverages ($\theta_0 \geq 0.9$) as estimated from the peak shape analysis (see below). The catalyst was then ramped to 1073 K at a linear heating rate of 25 K min^{-1} in flowing He (50 ml min^{-1}). Analysis of the effluent flow was done with a quadrupole mass spectrometer (VG 200 instrument).

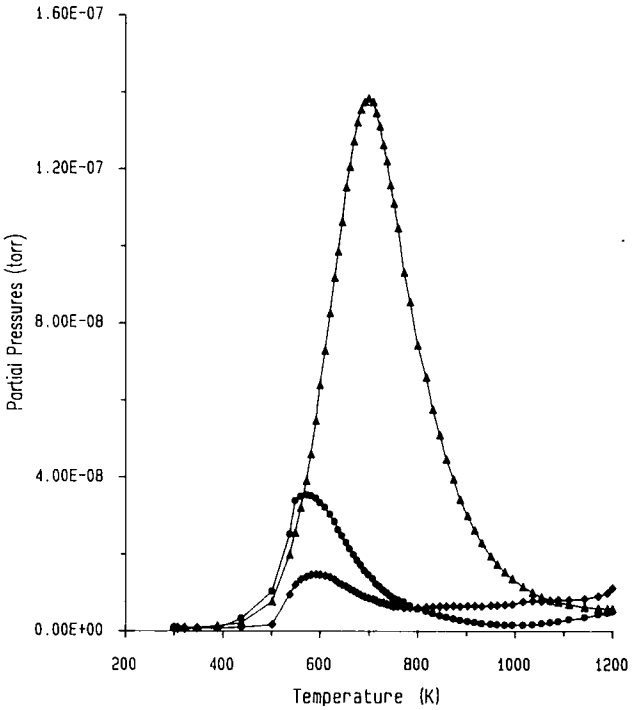

FIG. 1. A typical experiment of temperature-programmed desorption (TPD) of preadsorbed NO from a Rh/Al_2O_3 catalyst (sample D): ▲, N_2; ●, NO, and ◆, N_2O.

IR spectra were recorded on a Perkin–Elmer 983 instrument equipped with a Perkin–Elmer 3600 Data Station; 7–10 mg of the sample were pressed into thin wafers of approximately 1 cm^2 area. The measurements were carried out in the flow of reactants using a stainless-steel IR cell constructed according to Ref. (10).

RESULTS AND DISCUSSION

Temperature-Programmed Desorption of NO

Four species were detected in the thermal desorption experiments of adsorbed NO, namely, NO, N_2, N_2O, and O_2. Figure 1 shows a typical TPD spectrum for the nitrogen-containing products obtained from a NO-saturated catalyst. Oxygen, not shown, is evolved starting at about 1000 K (4, 11). The spectrum features broad bands with a single maximum for all the three nitrogen products desorbed. The NO peak appears at a temperature which is slightly lower than that of the N_2O peak. By contrast, the N_2 peak maximum appears at a temperature which is

about 100 K higher. This kind of behavior is common for all the samples investigated.

Generally speaking, nitrogen evolution in the TPD of preadsorbed NO shows two peaks: there is a β_1 peak centered at about 450–480 K and a β_2 peak centered at about 550–650 K which are attributed, respectively, to the following processes (4, 11, 12):

$$NO_a + N_a \longrightarrow N_2 + O_a + * \qquad \beta_1$$
$$N_a + N_a \longrightarrow N_2 + 2*. \qquad \beta_2$$

The temperature of the β_2 peak depends on the surface coverage (4, 11, 12), which is consistent with a second-order desorption process. On increasing surface coverage, the β_2 peak fills up first and it moves toward lower temperatures. At high coverages, most of the N_2 evolves as β_1, β_2 being almost negligible (11). Presence of a single peak for the N_2 evolution (Fig. 1) give rise to the question as to which process is operative in our experimental conditions.

Application of Gorte's criteria (13, 14) to our experimental conditions suggests that particle concentration gradients should be negligible for our catalysts. Therefore analysis of the TPD peaks by the method of Amenomiya and Cvetanovic (15) is applicable (13). For such analysis, Ibok and Ollis (16) suggested a useful criterion based on a peak shape index (S) which allows one to determine which kind of regime is operative, i.e., first- or second-order desorption, kinetically or thermodynamically controlled. Accordingly, we calculate a shape index (S) of 1.05 for the N_2 desorption peak in Fig. 1. This value is consistent with a second-order desorption with free readsorption occurring for the N_2 desorption feature. Moreover, the value of $S = 1.05$ is consistent with a high initial coverage of $\theta_0 = 0.9$ which is to be expected since a twofold excess of NO with respect to the exposed Rh was pulsed over the catalyst. The absence of the first-order desorption feature should be attributed to presence of free readsorption which shifts the peaks toward higher temperatures (17), thus favoring the high-temperature N_a recombination path (4, 11, 12). The attribution of the N_2 desorption feature to the second-order process is also consistent with the observation that over supported catalysts, the first-order desorption peak is generally observed in correspondence with the NO and N_2O desorption peaks (11).

The data obtained over the five samples investigated are illustrated in Fig. 2. Both the relative amount of evolved gas and the temperatures of peak maxima are significantly affected by the dispersion of the catalyst. As shown in Fig. 2a, peak temperatures for the desorbed products appear to be monotonically dependent on the catalyst dispersion. Smaller rhodium particle size shifts all three peaks significantly toward higher values. Notably, N_2 formation is strongly favored over evolution of NO and N_2O on increasing the particle size. This is illustrated in Fig. 2b.

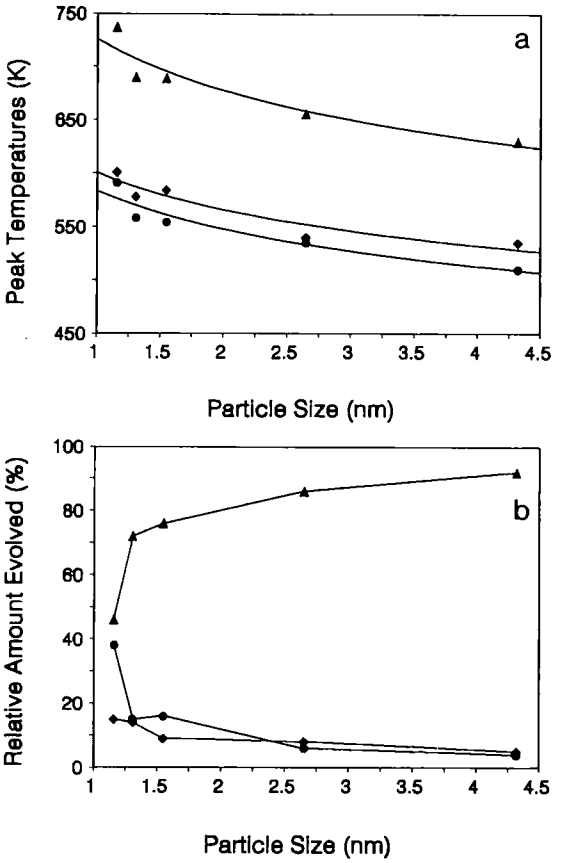

FIG. 2. TPD of preadsorbed NO from Rh/Al_2O_3 catalysts: dependences of peak temperatures (a) and relative amounts evolved (b) on particle size. Symbols as in Fig. 1.

It is interesting to compare the trends shown in Fig. 2 with the data reported by Altman and Gorte for Rh/α-$Al_2O_3\{0001\}$ model catalysts prepared by vacuum evaporation of Rh onto a sapphire surface (18). They also observed a shift of the high temperature N_2 peak toward higher temperatures upon increasing the dispersion from 22 to 42%. Such a behavior should be attributed to higher activation energies for the nitrogen recombination step. Noteworthy is that our results also show a strong enhancement of the NO dissociation on increasing particle size (Fig. 2b), which was not observed in the previous investigation (18). This could be attributed to the narrow range of dispersions, i.e., 22 to 42% investigated. On the other hand, it was observed that at room temperature only a small amount of adsorbed NO dissociates, while most of the NO dissociation occurs on increasing the temperature (11). Since we are operating in the presence of a free readsorption equilibrium, readsorption of NO is occurring, hence NO dissociation is favored.

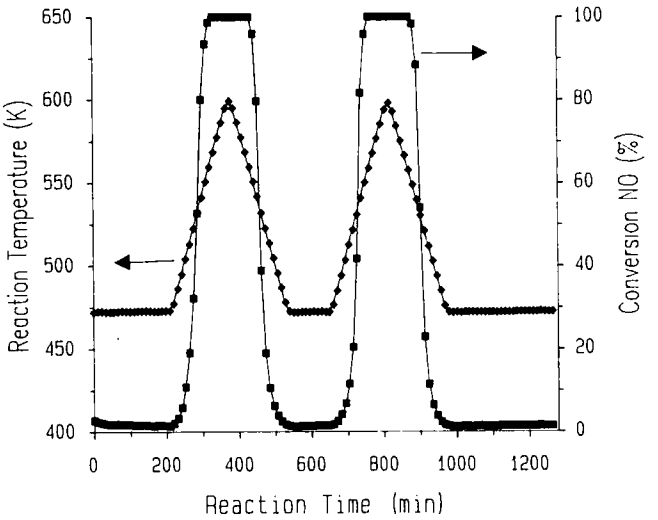

FIG. 3. NO conversion (■) and temperature profile (◆) over Rh/Al_2O_3 catalysts vs reaction time in a typical catalytic experiment (sample D).

Catalytic Experiments

Catalytic experiments were carried out in a flow reactor in the range of temperatures 473–700 K at GHSV of 50,000–100,000 h^{-1} using helium-diluted CO : NO = 3 : 1 mixture (see Experimental). Consistently with previous observations (2, 6), deactivation with time on stream of the freshly reduced catalysts was always observed. The catalysts were therefore aged at 473 K in the reaction conditions until steady-state conversions were attained, and afterward the catalysts were typically subjected to a testing cycle such as shown in Fig. 3. This allowed us to measure both the light-off temperatures (corresponding to 50% conversion) and turnover frequencies (at conversions lower than 10%), either in the course of the run-up or the run-down experiments. The symmetry of the conversion vs reaction time curve indicates that no appreciable deactivation of the catalysts occurs in the course of the temperature programme. Data obtained for all the samples investigated are reported in Table 2.

Light-off temperature (corresponding to 50% conversion) is often reported as a measure of the activity of a three-way catalyst (19, 20). However, it was recently pointed out by Cho (21) that, keeping the reaction parameters constant, i.e., space velocities and loading of the catalyst, the light-off temperature depends on metal dispersion. He showed that by assuming a rate equation for the NO conversion of the type (4)

$$r = k(T)f(c),$$

where $k(t)$ is the reaction rate constant for NO conversion which depends on the temperature and $f(c)$ represents the remaining factor of the rate equation which depends on surface coverages, then, upon assumption of an Arrhenius type dependence of reaction rate on temperature, the following expression for the light-off temperatures can be derived (for a detailed derivation of Eq. [1], compare Ref. (21)):

$$1/T_2 - 1/T_1 = (R/E_a)\ \ln[(Rh_s/F)_2 f_2(c)/(f_1(c)(Rh_s/F)_1)]. \quad [1]$$

(Rh_s = exposed rhodium (mol); F = total flow rate (ml min^{-1}).)

This equation shows that for the same reaction conditions, the light-off temperatures depend on rhodium dispersion. Cho suggested that $f(c)$ is independent of the temperature (21). We measured for the sample E light-off temperatures of 508 ± 2 K and 524 ± 2 K using $Rh_s/F = 3.70 \times 10^{-7}$ and 1.26×10^{-7} mol min ml^{-1} respectively. Therefore, by assuming $f_1(c) = f_2(c)$ and an activation energy of 35 kcal/mol (Table 2), from the former value, a light-off temperature of 524 K can be calculated from Eq. [1] for a $Rh_s/F = 1.26 \times 10^{-7}$ mol min ml^{-1}. This confirms the independence of $f_1(c)$ on the temperature in the range of temperatures investigated. This observation also shows that light-off temperature can be used as a straight measure of catalyst activity as long as a constant Rh_s/F ratio is employed. Consequently, all the measurements reported in Table 2 were carried out using a constant $Rh_s/F = 1.26 \times 10^{-7}$ mol min ml^{-1}. In this way, any change in the light-off temperature should be attributed to a variation of specific activity of the metal particles.

A perusal of the light-off temperatures reported in Table 2 does not bring out any clear relationship among them and the catalyst dispersions or calculated particle diameters. Over the catalysts employed, two distinct regimes, characterized by different apparent activation energies were always observed (compare Table 2). Notably, the inflection point of the Arrhenius plot occurs at 498 ± 4 K independently of the sample employed. At higher temper-

TABLE 2

NO Reduction by CO over Rh/Al_2O_3 Catalysts

Sample code	E'_a	E''_a	T.N. (503 K)	T.N. (473 K)	Light-off temp. (K)
A	25	35	4.1×10^{-3}	5.5×10^{-4}	538
B	14	28	4.8×10^{-3}	1.6×10^{-3}	546
C	20	30	4.5×10^{-3}	1.2×10^{-3}	545
D	22	31	8.4×10^{-3}	1.7×10^{-3}	532
E	30	35	1.4×10^{-2}	1.4×10^{-3}	524

Note. E'_a, apparent activation energy (kcal/mol) measured below 498 K; E''_a, apparent activation energy (kcal/mol) measured above 498 K; and T.N., (moles of NO converted) (moles Rh exposed)$^{-1}$ s^{-1}.

atures, higher activation energies are observed. Such changes of activation energies were previously observed over dispersed catalysts and they are generally attributed to a shift in the rate-determining step from the NO dissociation to either the N_a recombination step (3, 6) or the reaction of CO with adsorbed oxygen (7). Generally speaking, for dispersed catalysts, higher apparent activation energies for the CO + NO reaction are found as compared with the single Rh crystals which are characterized by a single activation energy (1). Thus, Oh and Eickel (3) reported activation energies of 30, 32 and 39, 37 kcal/mol for a 100 and 26% dispersed catalyst, respectively, in the low- and high-temperature range. Less dispersed catalysts showed even lower activation energies. By contrast, Pande and Bell reported E_a = 24 kcal/mol for a 64% dispersed Rh/Al_2O_3 (22). For a 61% dispersed catalyst, E_a of 28 kcal/mol was observed (6). In another investigation, 46 kcal/mol was found for a 12% dispersed catalyst (1). Definitely, there are scattered values reported in the literature and this is the case also for the data reported in Table 2. All these results suggest that evolution of the catalyst occurs upon variation of the reaction temperature (see below).

The turnover numbers for NO conversion (Table 2) are therefore reported both at 503 and 473 K, i.e., in regions characterized by different E_a. A comparison of the data reported in Table 2 shows that at 503 K, the specific activity of rhodium is effectively increased by an increase of particle size. At variance with this, such behavior is not apparent at 473 K. In summary, from the data reported in Table 2, it appears that promotional effects of particle size on catalytic properties of rhodium in the range of dispersion (D = 25–95%) are heavily influenced by the reaction conditions and, particularly, by the reaction temperature.

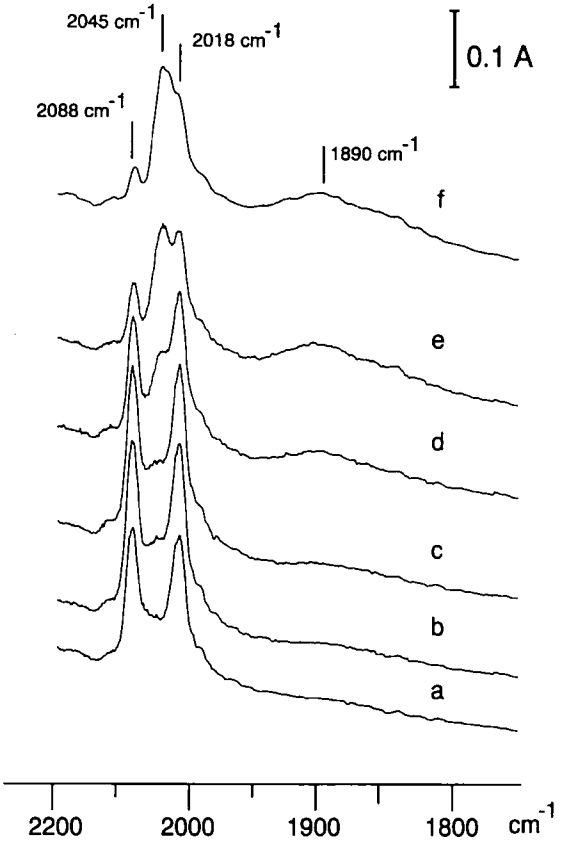

FIG. 4. IR spectra in the ν(CO) region of sample D in flowing CO (3% in He) at 473 K after respectively 1 min (a), 5 min (b), 10 min (c), 30 min (d), 60 min (e), and (f) after 1 min following desorption of adsorbed CO in flow of He for 120 min at 473 K.

IR Measurements

In order to obtain an insight on changes in the catalyst in the reaction conditions, *in situ* IR measurements were carried out over the samples investigated. The interaction of CO with supported Rh has been a subject of intensive research in the past. At present, there is a substantial agreement on the attribution of the IR bands at 2040–2080 and at about 1850 cm^{-1} respectively to linear and bridged carbonyl species adsorbed on a contiguous Rh(0) surface, while the bands at 2080–2100 and 2020–2030 cm^{-1} are associated respectively with the symmetric and asymmetric stretch of a *gem*-dicarbonyl $Rh^I(CO)_2$ species (23–26). It was also suggesed that formation of Rh^I occurs through oxidation of the metal particles by surface OH groups in the presence of CO (27). This was confirmed by careful IR (28), XPS, and EXAFS (29) studies. The effect of CO on the morphology of rhodium particles is twofold. At 300–400 K, on an Al_2O_3 support, CO adsorption leads to oxidative disruption of rhodium particles as detected by the presence of bands at 2020–2030 and 2080–2100 cm^{-1}, while above 423 K, it leads to a reductive agglomeration of the metal particles and formation of bands due to linear and bridged carbonyls (26). It is worth noting that, while the former process is quite fast, the latter is quite slow. Thus, in principle, by carrying out the CO adsorption at an appropriate temperature, where the reductive agglomeration occurs slowly, a time-resolved spectroscopy could give direct indication of the actual Rh morphology in the catalyst. Figure 4 shows the effects on CO adsorption in flow conditions at 473 K on the IR spectra of the sample D (D = 41%) as a function of time.

After 1 min, bands at 2088 and 2018 cm^{-1} attributable to the geminal dicarbonyl and perhaps a weak shoulder at 2045 cm^{-1} attributable to the linear CO appear. The intensity of the bands grows with time and with, apparently, no significant variations in the relative intensities of the ν(CO) bands up to 5 min of adsorption (Fig. 4, spectra a–b). Subsequently, the reductive agglomeration

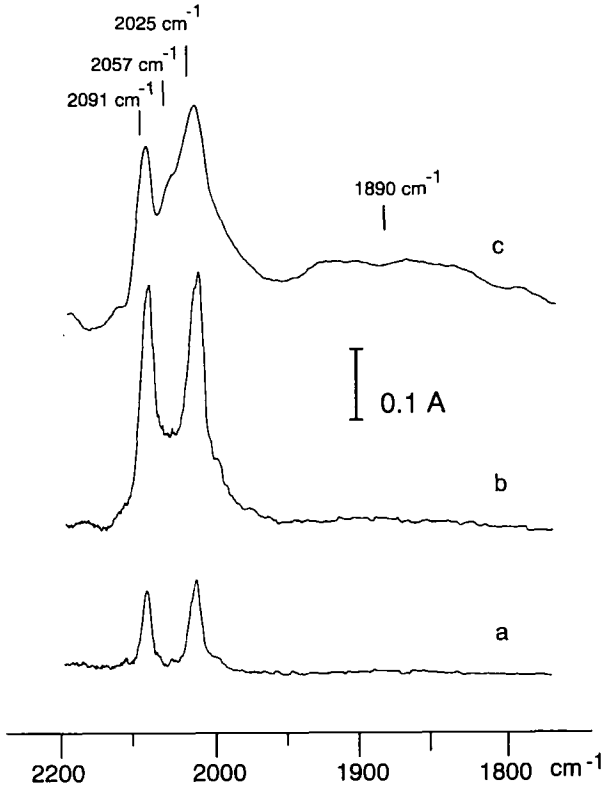

FIG. 5. IR spectra in the ν(CO) region measured after 1 min in flowing CO (3% in He) at 473 K of sample A (a), sample D (b), and sample E (c).

of rhodium particles occurs as shown by the increase of the intensity of the band at 2045 cm^{-1} (linear carbonyl) and the appearance of the band at 1890 cm^{-1} due to bridged CO (Fig. 4, spectrum d). Significantly, when CO is desorbed in a flow of helium at 473 K from an agglomerated sample (Fig. 4, spectrum e), upon readsorption of CO, the sample still shows typical features of agglomerated catalyst as shown in the spectrum f of Fig. 4 which was collected after 1 min in flowing CO. Conversely, readsorption of CO at room temperature over a similarly agglomerated catalyst gives a spectrum with only geminal dicarbonyl features. The higher degree of the agglomeration shown in spectrum f compared to spectrum e should be associated with further agglomeration occurring during the CO desorption, which is a slow process (26). Therefore, this experiment shows that, by CO adsorption at 473 K, the morphology of the surface rhodium particles can be easily detected.

Figure 5 shows the IR spectra in the ν(CO) region taken at 473 K after 1 min in flowing CO of the samples A (D = 95%), D (D = 41%), and E (D = 25%). The general appearance of the three spectra is consistent with the chemisorption measurements; higher loadings and hence lower dispersions favor appearance of linear and bridged features (30).

In order to obtain insight into the nature of the catalyst in reaction conditions, a freshly reduced sample D was treated at 473 K in the presence of flowing CO and NO using the same W/F as that employed in the catalytic conditions. After aging the catalyst for 2 hours in reaction conditions, spectrum a of Fig. 6 was obtained, which shows bands at 2167, 2091, 2022, and 1896 cm^{-1}, and a weak shoulder at 2145 cm^{-1}. Such a picture is consistent with a previous report (31), and accordingly we assign the bands as follows: 2091 and 2022 cm^{-1} to $Rh^{I}(CO)_2$ (23–31), 2167 cm^{-1} to Rh–NCO, 2045 cm^{-1} to Rh–CN, and 1896 cm^{-1} to $Rh–NO^{\delta+}$ (31–35). However, as suggested by a referee, the bands at 2167 and 1896 cm^{-1} could be alternatively assigned to a mixed Rh(NO)(CO) species, in view of the observation that Rh–NCO appeared thermally unstable (36). On increasing the reaction temperature, the overall intensity of the bands decreases as desorption processes are favored, while a new band at 2254 cm^{-1} is observed whose intensity increases with temperature (Fig. 6, spectra c, e). This band is attributed to a –NCO species bound to the alumina (31, 33). Varia-

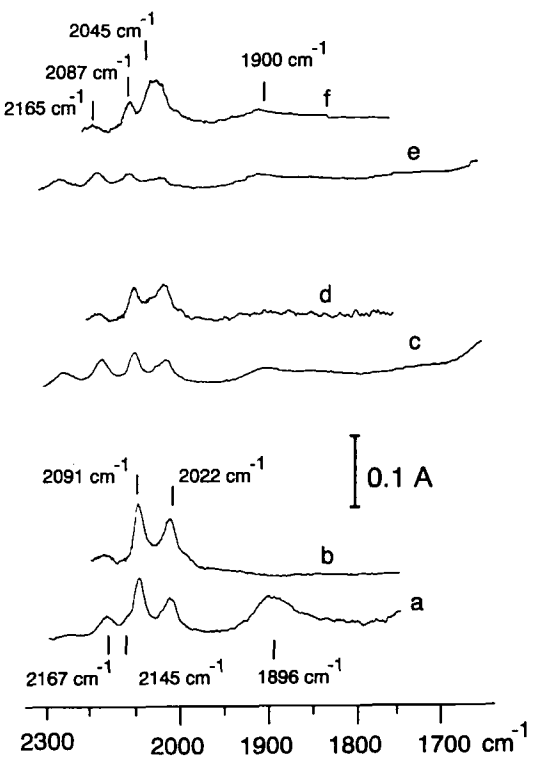

FIG. 6. IR spectra of sample D after aging in the presence of CO and NO in reaction conditions at respectively 473 K (a), 503 K (c) and 523 K (e); (b), (d), and (f) are the corresponding spectra after 1 min in flowing CO (3% in He) at 473 K following desorption of the products in flow of He for 2 h at the reaction temperature.

tion of its intensity with temperature is consistent with a migration of the isocyanate species to the support (31, 34).

Desorption of the products from the sample in flowing helium at 473 K and subsequent CO readsorption produced spectrum b of Fig. 6 which shows essentially the two bands due to the rhodium dicarbonyl. The absence of the bridged feature and the fact that only a weak, if any, band due to the linear CO is observed, indicates that at 473 K, in the presence of NO, the reductive agglomeration of the rhodium particles does not occur. Consistently, Solymosi *et al.* have shown that in the presence of NO, the reductive agglomeration of rhodium particles is strongly inhibited (36).

Noteworthy is that on increasing the reaction temperature, a progressive agglomeration of rhodium particles, starting at about 500 K, becomes clearly apparent as the linear feature at 2045 cm^{-1} is strongly increased compared to the spectrum b of Fig. 6 and it now clearly appears as a shoulder at 2048 cm^{-1} (Fig. 6, spectrum d).

Finally, after carrying out the reaction at 523 K, an IR spectrum of a fully agglomerated catalyst featuring bands at 2087, 2045 and 1900 cm^{-1} was obtained (Fig. 6, spectrum f). Similar results were obtained also with the other samples.

On the basis of these observations, the data reported in Table 2 can be rationalized as follows. Due to the migration of rhodium on the alumina surface, particle size continuously changes as a function of the temperature. Consequently, the apparent activation energies are related to catalysts whose nature continuously changes with temperature due to different agglomeration/disruption processes, depending on the sample. It should be noted, however, that in our reaction conditions, the agglomeration/disruption process appears to be relatively faster compared to the heating/cooling rate (0.8 K/min) employed, since the inflection point in the Arrhenius plot is equal within experimental error both for the run-up and run-down experiments.

The unprecedented observation that the agglomeration process starts occurring at a temperature which is close to that of the inflection point in the Arrhenius plot strongly suggests that the shift in the rate-determining step, which was associated with the variation of activation energies (3, 6), is due to a CO induced reconstruction of rhodium particle morphology. This is also supported by preliminary experiments we have carried out on a rhodium foil which showed no such inflection point in the Arrhenius plot.

As far as the turnover numbers are concerned, the promoting effects of the particle size are observed only above 500 K, where the agglomeration prevails. This is consistent with the promotional effect of the particle size on the NO dissociation and N_2 formation, shown by the TPD. The N_a recombination step (β_2) is generally believed to be the rate-determining step over dispersed catalysts (3, 6). Therefore in the presence of agglomerated particles, both NO dissociation and N_a recombination are promoted so that the amount of N_a formed increases with particle size which results in an overall reaction rate enhancement. Below 500 K, CO induced oxidative disruption is operative, and therefore the promotional effect of the particle size on NO dissociation is not effective and no enhancement of catalytic activity is indeed observed. These results stress the necessity of contiguous rhodium surface to enhance NO dissociation and hence catalytic activity. Consistently, the activity of Rh(111) was some 2000 times higher than that of the dispersed catalyst (1). However, the magnitude of the rate enhancement observed here suggests that other factors must also play a role in determining the specific activity of the supported catalysts, besides a preferential formation of, e.g., Rh(111) planes which might be expected on increasing particle size. Finally, keeping in mind the results of the IR measurements it appears clearly that conclusions on the specific activity, based on the turnover numbers only, should be taken with extreme care because of the continuous changes of the particle morphology. However, very recently Rasband and Hecker observed a very good agreement between the rhodium dispersions as measured by H_2 chemisorption and by IR absorption in the ν(CO) region over agglomerated catalysts (37). This strongly suggests that only the turnover numbers measured over agglomerated catalysts are fully significant.

CONCLUSIONS

The data reported here show that the reaction rates for the NO reduction by CO are enhanced by an increase of the size of the rhodium particles for particles of intermediate dispersions (25–95%). However, the promotion effects appear to be strongly dependent on the reaction temperature. Since, below 500 K, the CO induced oxidative disruption of the rhodium particles appears to regulate the rhodium particle size, no reaction rate promotion is obtained. On the other hand, above 500 K, reductive agglomeration of the rhodium particles occurs. This phenomenon is suggested to be responsible for the observed changes in the activation energy which might be related to a shift of the r.d.s. to the N_2 recombination path (3, 6). As shown by TPD, the N_2 recombination is strongly favored by increasing the particle size and hence enhancement of catalytic activity is observed.

The results stress the importance of a proper rhodium particle size for obtaining a highly active catalyst. Moreover, they indicate that it would be highly desirable to stabilize the rhodium dispersion in the catalytic conditions. Recently, Paul *et al.* reported that by silanization of surface OH groups, rhodium dispersions are stabilized against oxidative disruption (38, 39).

ACKNOWLEDGMENTS

We thank Professor Renzo Rosei for helpful discussion and Mr. Elvio Merlach for technical help. Financial support from the Ministero dell'Università e della Ricerca Scientifica (Rome) and from C.N.R. Rome under "Progetto Finalizzato Chimica Fine II" and "Comitato Scienze Technologiche e Innovazioni" is also acknowledged.

REFERENCES

1. Oh, S. H., Fisher, G. B., Carpenter, J. E., and Goodman, D. W., *J. Catal.* **100,** 360 (1986).
2. Hecker, W. C., and Breneman, R. B., *in* "Catalysis and Automotive Pollution Control" (A. Crucq and A. Frennet, Eds.), p. 257. Elsevier, Amsterdam, 1987.
3. Oh, S. H., and Eickel, C. C., *J. Catal.* **128,** 526 (1990).
4. Campbell, C. T., and White, J. M., *Appl. Surf. Sci.* **1,** 347 (1978).
5. Hecker, W. C., and Bell, A. T., *J. Catal.* **84,** 200 (1983).
6. Oh, S. H., *J. Catal.* **124,** 477 (1990).
7. Cho, B. K., Shanks, B. H., and Bailey, J. E., *J. Catal.* **115,** 486 (1989).
8. Villarubia, J. S., and Ho, H., *J. Chem. Phys.* **87,** 750 (1987).
9. Anderson, J. R., "Structure of Metallic Catalysts." Academic Press, London, 1975.
10. Hicks, R. F., Kellner, C. S., Savatsky, B. J., Hecker, W. C., and Bell, A. T., *J. Catal.* **71,** 218 (1981).
11. Chin, A. A., and Bell, A. T., *J. Phys. Chem.* **87,** 3700 (1983).
12. Root, T. W., and Schmidt, D. L., *Surf. Sci.* **134,** 30 (1983).
13. Gorte, R. J., *J. Catal.* **75,** 164 (1982).
14. Demmin, R. A., and Gorte, R. J., *J. Catal.* **90,** 32 (1984).
15. Cvetanovic, R. J., and Amenomiya, Y., *Adv. Catal.* **17,** 103 (1967); Cvetanovic, R. J., and Amenomiya, Y., *Catal. Rev.* **6,** 21 (1972).
16. Ibok, E. E., and Ollis, D. F., *J. Catal.* **66,** 391 (1980).
17. Rieck, J. S., and Bell, A. T., *J. Catal.* **85,** 143 (1984).
18. Altman, E. I., and Gorte, R. J., *J. Catal.* **113,** 185 (1988).
19. Engler, B., Koberstein, E., and Schubert, P., *Appl. Catal.* **48,** 71 (1989).
20. Cho, B. K., and West, L. A., *Ind. Eng. Chem. Res.* **25,** 158 (1986).
21. Cho, B. K., *J. Catal.* **131,** 74 (1991).
22. Pande, N. K., and Bell, A. T., *J. Catal.* **98,** 7 (1986).
23. Yang, A. C., and Garland, C. W., *J. Phys. Chem.* **61,** 1504 (1957).
24. Worley, S. D., Rice, C. A., Mattson, G. A., Curtis, C. W., Guin, J. A., and Tarrer, A. R., *J. Phys. Chem.* **76,** 20 (1982).
25. Yates, J. T., Duncan, T. M., Worley, S. D., and Vaughan, R. W., *J. Phys. Chem.* **70,** 1219 (1979).
26. Solymosi, F., and Pasztor, M., *J. Phys. Chem.* **89,** 4789 (1985).
27. Smith, A. K., Hughes, F., Theolier, A., Basset, J. M., Ugo, R., Zanderighi, G. M., Bilhou, G. M., Bilhou-Bougnol, V., and Graydon, V. F., *Inorg. Chem.* **18,** 3104 (1979).
28. Basu, P., Panayotov, D., and Yates, J. T., *J. Am. Chem. Soc.* **110,** 2074 (1988).
29. Van't Blik, H. F. J., van Zon, J. B. A. D., Huizing, T., Vis, J. C., Koningsberger, D. C., and Prins, R., *J. Am. Chem. Sco.* **107,** 3139 (1985).
30. Cavanagh, R. R., and Yates, J. T., *J. Phys. Chem.* **74,** 4150 (1981).
31. Dictor, R., *J. Catal.* **109,** 89 (1988).
32. Arai, H., and Tominaga, H., *J. Catal.* **43,** 131 (1976).
33. Hyde, E. A., Rudham, R., and Rochester, C. H., *J. Chem. Soc. Faraday Trans. 1,* **80,** 531 (1984).
34. Hecker, W. C., and Bell, A. T., *J. Catal.* **85,** 389 (1984).
35. Unland, M. L., *J. Phys. Chem.* **77,** 1952 (1973).
36. Solymosi, F., Bansagi, T., and Novak, E., *J. Catal.* **112,** 183 (1988).
37. Rasband, P. B., and Hecker, W. C., *J. Catal.* **139,** 551 (1993).
38. Paul, D. K., Ballinger, T. H., and Yates, J. T., *J. Phys. Chem.* **94,** 4617 (1990).
39. Paul, D. K., and Yates, J. T., *J. Phys. Chem.* **95,** 1699 (1991).